C–H Activation

International Edition: DOI: 10.1002/anie.201507933
German Edition: DOI: 10.1002/ange.201507933

A Highly Reactive Seven-Coordinate Osmium(V) Oxo Complex: $[Os^{V}(O)(qpy)(pic)Cl]^{2+}$

*Yingying Liu, Siu-Mui Ng, William W. Y. Lam, Shek-Man Yiu, and Tai-Chu Lau**

Abstract: *Seven-coordinate ruthenium oxo species have been proposed as active intermediates in catalytic water oxidation by a number of highly active ruthenium catalysts, however such species have yet to be isolated. Reported herein is the first example of a seven-coordinate group 8 metal-oxo species, $[Os^{V}(O)(qpy)(pic)Cl]^{2+}$ (qpy = 2,2′:6′,2″:6″,2‴-quaterpyridine, pic = 4-picoline). The X-ray crystal structure of this complex shows that it has a distorted pentagonal bipyramidal geometry with an Os=O distance of 1.7375 Å. This oxo species undergoes facile O-atom and H-atom-transfer reactions with various organic substrates. Notably it can abstract H atoms from alkylaromatics with C–H bond dissociation energy as high as 90 kcal mol^{-1}. This work suggests that highly active oxidants may be designed based on group 8 seven-coordinate metal oxo species.*

High-valent metal oxo complexes play important roles as oxidants in both chemical and biological systems.[1–4] Extensive work has been done on oxidation by metal oxo complexes, especially those based on iron[5] and ruthenium,[6] because, with a suitable choice in ancilliary ligands these metals can form highly oxidizing oxo complexes. In contrast, osmium oxo species are in general much less oxidizing than either ruthenium or iron oxo species.[7] Apart from the use of OsO_4[8] and *cis*-$[Os^{V}(O)(OH)]$ species[9] in the *cis* dihydroxylation of alkenes, there are few reports on C–H bond activation based on osmium oxo species.

So far all known group 8 metal oxo complexes are eiher four-, five-, or six-coordinate species. However, recently seven-coordinate ruthenium(V) oxo species have been proposed as active intermediates in the catalytic oxidation of water[10–12] and organic substrates[13–15] in the presence of a number of octahedral ruthenium catalysts. So far no such species has been isolated, although a seven-coordinate Ru^{IV}–OH species, which is probably a catalytic resting state, has been isolated by Sun and co-workers.[11a] In contrast, seven-coordinate osmium oxo species should be more stable and hence may be more readily isolated. We report herein the synthesis, structure, and reactivity of the first seven-coordinate osmium oxo complex, $[Os^{V}(O)(qpy)(pic)Cl]^{2+}$ (qpy = 2,2′:6′,2″:6″,2‴-quaterpyridine; pic = 4-picoline). This complex is a strong oxidant. It undergoes facile O-atom and H-atom-transfer reactions with various organic substrates.

The synthesis of the [Os(qpy)] complexes is summarized in Scheme 1. Reaction of $(NH_4)_2OsCl_6$ with 1 equivalent of

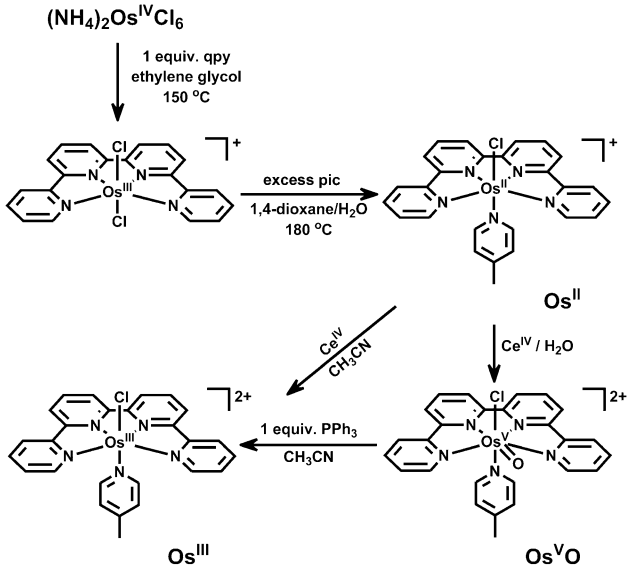

Scheme 1. Synthesis of seven-coordinate osmium(V) oxo species.

qpy in ethylene glycol at 150 °C afforded the purple $[Os^{III}(qpy)Cl_2]^{+}$, isolated as the ClO_4^- salt. Refluxing $[Os^{III}(qpy)Cl_2]^{+}$ with 10 equivalents of 4-picoline in 1,4-dioxane/water (4:1) under argon for 20 hours resulted in the formation of the green complex $[Os^{II}(qpy)(pic)Cl]^{+}$ (**Os^{II}**), isolated as the PF_6^- salt (Scheme 1). Oxidation of **Os^{II}** with 40 equivalents of $(NH_4)_2[Ce(NO_3)_6]$ (CAN) gave the dark-red seven-coordinate osmium(V) oxo complex $[Os^{V}(qpy)(pic)Cl(O)]^{2+}$ (**$Os^{V}O$**), isolated as the PF_6^- salt. Treatment of **$Os^{V}O$** with 1 equivalent of PPh_3 in CH_3CN afforded the dark brown Os^{III} complex $[Os^{III}(qpy)(pic)Cl]^{2+}$ (**Os^{III}**). Direct oxidation of **Os^{II}** with CAN also gave **Os^{III}**, but the product was usually contaminated with a small amount of either **Os^{II}** or **$Os^{V}O$**.

All newly synthesized compounds have been characterized by elemental analysis, electrospray ionization mass spectrometry (ESI/MS), and infrared spectroscopy (IR), as well as either nuclear magnetic resonance (NMR) spectroscopy or magnetic susceptibility measurements. **Os^{II}** is diamagnetic, as expected for its low-spin d^6-electronic configuration, while **Os^{III}** and **$Os^{V}O$** are paramagnetic with $S = {}^1/_2$ ($\mu_{eff} = 2.20$ and 2.05 μ_B, respectively, Evans' method). The ESI/MS of **Os^{II}**, **Os^{III}**, and **$Os^{V}O$** in CH_3CN show the parent peaks at $m/z = 630.5$, 315, and 323, respectively. In the IR

[*] Y. Liu, Dr. S. M. Ng, Dr. W. W. Y. Lam, Dr. S. M. Yiu, Prof. T. C. Lau
Department of Biology and Chemistry and Institute of Molecular Functional Materials, City University of Hong Kong
Tat Chee Avenue, Kowloon Tong, Hong Kong (China)
E-mail: bhtclau@cityu.edu.hk

Supporting information for this article is available on the WWW under http://dx.doi.org/10.1002/anie.201507933.

spectrum of **Os^{V}O**, the ν(Os=O) stretch occurs at 856 cm^{-1}, and this peak is shifted to 816 cm^{-1} (theoretical 811 cm^{-1}) upon ^{18}O-labeling (see Figure S1 in the Supporting Information). This ν(Os=O) stretch value is similar to that of the octahedral Os^{V}=O species [Os^{V}(O)(OH)(tpa)]$^{2+}$ [881 cm^{-1}; tpa = tris(2-pyridylmethyl)amine].[9a]

The molecular structures of **Os^{II}**(PF$_6$), **Os^{III}**(PF$_6$)$_2$, and **Os^{V}O** (PF$_6$)$_2$ have also been determined by X-ray crystallography (Figure 1). The X-ray crystal structure of **Os^{II}**(PF$_6$) (Figure 1a; see Table S1) shows that the osmium complex has a distorted octahedral geometry with the equatorial positions occupied by the four N atoms of the planar qpy ligand, and the axial positions occupied by the picoline and the chloro ligands. The two inner Os-N(qpy) distances (Os1-N3 = Os1-N3a = 1.9349 Å) are significantly shorter (by 0.185 Å) than the two outer ones (Os1-N2 = Os1-N2a = 2.1201 Å), as a result of considerable strain in the planar coordination mode of the "short" qpy ligand. Notably, the complex has a large N2-Os1-N2a bite angle of 121.655°, thus suggesting that it is possible to accommodate an additional small ligand such as oxo.

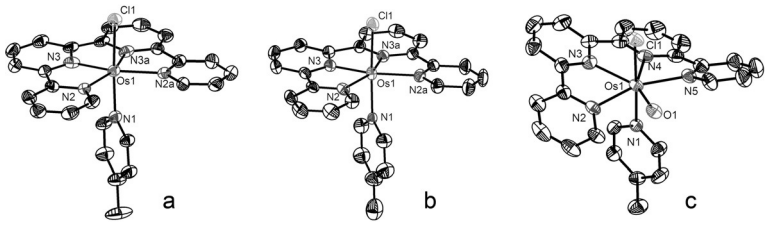

Figure 1. ORTEP drawings of a) **Os^{II}**, b) **Os^{III}**, and c) **Os^{V}O**. Thermal ellipsoids are drawn at 50% probability. Anions, solvent, and hydrogen atoms are omitted for clarity. In (a) and (b), symmetry operations used to generate equivalent atoms are (+*x*, +*y*, −*z*+1/2) and (+*x*, −*y*, +*z*), respectively.

The bond distances and angles for **Os^{III}** are comparable to those of **Os^{II}** (Figure 1b; see Table S2), which is attributed to strong π-back bonding between Os^{II} and the qpy and pic ligands.

The X-ray crystal structure of **Os^{V}O**(PF$_6$)$_2$ (Figure 1c; see Table S3) shows that it is a seven-coordinate osmium(V) oxo species with a distorted pentagonal bipyramidal geometry. The equatorial positions are occupied by the four N atoms of the quaterpyridine ligand and an oxo ligand, while the axial positions are occupied by a picoline and a chloro ligand. The N2-Os1-N5 bite angle is expanded to 154.161° after accommodating the new oxo ligand. The Os=O (Os1-O1) distance of 1.7375 Å is comparable to that of six-coordinate osmium(V) oxo complex [Os^{V}(O)(OH)(tpa)]$^{2+}$ (1.726 Å) as reported in the literature.[9a]

Os^{V}O is unstable in water (see Figure S2), and ESI/MS shows the appearance of peaks resulting from the loss of 4-picoline within minutes upon dissolution in water (see Figure S3). However, it is stable in CH$_3$CN for more than 8 hours at room temperature, as monitored by UV/Vis spectrophotometry (see Figure S4).

The cyclic voltammetry (CV) of **Os^{II}** and **Os^{III}** exhibit a reversible Os$^{III/II}$ couple at 0.42 V (versus SCE, $\Delta E = 61$ mV; Figure 2a). An irreversible wave also occurs at 1.59 V, which presumably results from Os^{III}→Os^{IV}. This wave is accompanied by new reduction waves at 0.73 and 0.16 V, probably arising from decomposition of the Os^{IV} species (see Figure S5). The CV of **Os^{V}O** shows an irreversible wave at 0.27, and two quasi-reversible couples at −0.27 V and −0.53 V versus SCE (Figure 3b). The observed initial irreversible reduction wave, which probably results from Os^{V}O→Os^{IV}O, suggests that Os^{IV}O is unstable. This assumption is supported by the following experiment. **Os^{V}O** was treated with 1 equivalent of the one-electron reductant [Fe(Cp)$_2$] in CH$_3$CN, thus leading to an immediate color change from red to brown, most likely because of reduction of Os^{V}O to Os^{IV}O. ESI/MS of the product solution shows the presence of [Os^{IV}(O)(qpy)]$^{2+}$ and [Os^{IV}(O)(qpy)Cl]$^{+}$ at m/z = 259 and 553, respectively. There are also several minor peaks in the MS (see Figure S6). These results indicate that Os^{IV}O is unstable with respect to ligand dissociation and possibly other decomposition pathways. The subsequent quasi-reversible couples in CV of **Os^{V}O** are presumably a result of the additional reduction of

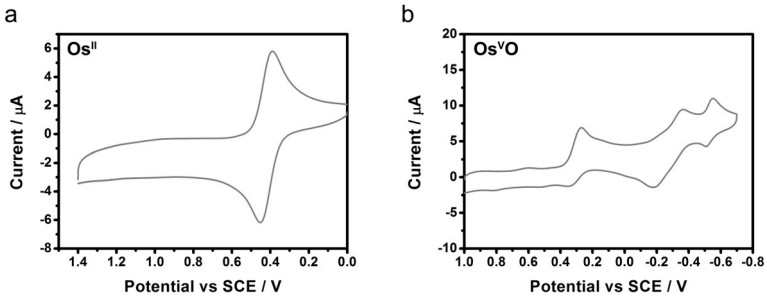

Figure 2. CV of a) 1.0 mM **Os^{II}** at 23 °C and b) 0.5 mM **Os^{V}O** at 0 °C in 0.1 M nBu$_4$NPF$_6$ in CH$_3$CN. Scan rate = 100 mV s^{-1}.

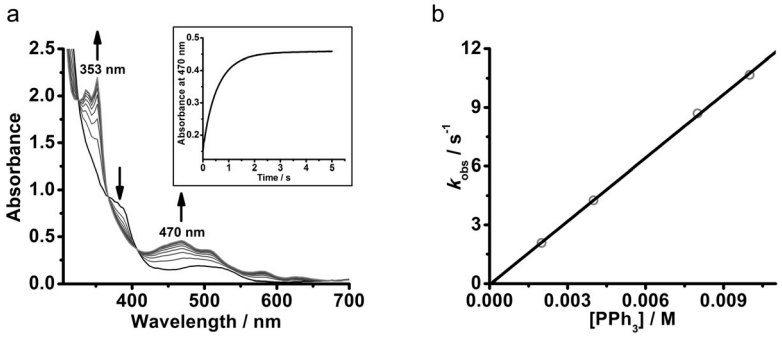

Figure 3. a) Spectral changes at 0.2 s intervals for the reaction between **Os^{V}O** (1.73×10^{-4} M) and PPh$_3$ (1.50×10^{-3} M) in CH$_3$CN at 298.0 K. Inset shows the corresponding absorbance–time trace at 470 nm. b) Plot of k_{obs} vs. [PPh$_3$]. Slope = $(1.08\pm0.02)\times10^{3}$; y-intercept = $-(6.33\pm10.6)\times10^{-2}$; r^2 = 0.9994.

$Os^{IV}O$ to Os^{III} and Os^{II} species, but the exact composition of these species are uncertain.

Unlike the corresponding ruthenium complexes, **$Os^{V}O$** does not oxidize water either stoichiometrically or catalytically using CAN. However, **$Os^{V}O$** readily oxidizes various organic substrates in CH_3CN, and reacts cleanly and rapidly with PPh_3, as monitored by UV/Vis spectrophotometry (Figure 3). The final spectrum indicates quantitative formation of **Os^{III}**. PPh_3O could be detected by GC/MS and ESI/MS [as $(PPh_3O + H)^+$, $m/z = 279$]. When ^{18}O-enriched **$Os^{V}O$** was used, $PPh_3{}^{18}O$ could be detected (see Figure S7). These results demonstrate O-atom transfer from **$Os^{V}O$** to PPh_3. The reaction is first-order in [**$Os^{V}O$**] and [PPh_3], and the second-order rate constant $k_2(PPh_3) = (1.08 \pm 0.02) \times 10^3\,M^{-1}s^{-1}$ at 298.0 K. A similar O-atom-transfer reaction occurs between **$Os^{V}O$** and thioanisole, and $k_2(PhSCH_3)$ was found to be $(9.29 \pm 0.13) \times 10^{-3}\,M^{-1}s^{-1}$ at 298.0 K (see Figures S8 and S9). **$Os^{V}O$** also undergoes O-atom transfer to cyclooctene to give cyclooctene oxide (yield 40%) with $k_2(C_8H_8) = (1.14 \pm 0.05) \times 10^{-4}\,M^{-1}s^{-1}$ (see Figure S10). These results show that **$Os^{V}O$** can react by a two-electron O-atom transfer pathway, which bypasses the unstable Os^{IV} state.

$Os^{V}O$ also reacts readily with various alkylaromatic compounds (RH) at ambient conditions. Oxidation of 1,10-dihydroanthracene (DHA) produces anthracene in 88% yield, while oxidation of cumene and diphenylmethane give the alcohol (44% yield) and ketone (76% yield), respectively (see Table S4). The yields are based on **$Os^{V}O$** functioning as a two-electron oxidant. However **$Os^{V}O$** does not react with alkanes. Kinetic studies have been carried out with a variety of alkylaromatic substrates (Figure 4; see Figures S11 and S12). The reactions are first-order in [**$Os^{V}O$**] and [RH]. The second-order rate constants span over six orders of magnitude. Xanthene, which has the smallest α C–H bond dissociation energy (BDE) of 75.5 kcal mol^{-1}, is the most reactive substrate [$k_2 = (3.65 \pm 0.14)\,M^{-1}s^{-1}$ at 298.0 K], while toluene, with the largest BDE of 89.8 kcal mol^{-1}, is least reactive [$k_2 = (1.05 \pm 0.01) \times 10^{-5}\,M^{-1}s^{-1}$]. The plot of $\log k'_2$ (rate constant per active H) versus C–H BDE of the alkylaromatic compounds is linear (slope = 0.43; Figure 5), and consistent with a mechanism involving initial rate-limiting H-atom transfer (HAT) from the alkylaromatic substrate to **$Os^{V}O$** ($Os^{V}O + R{-}H \rightarrow Os^{IV}OH + R^{\bullet}$), with subsequent rapid O-rebound ($Os^{IV}OH + R^{\bullet} \rightarrow Os^{III} + ROH$), as observed in C–H activation by cytochrome P450 and other metal oxo species.[16] The Os^{III} product could be detected by ESI/MS (see Figure S13). The product yields and rates were not affected by the presence of air or a radical scavenger such as $BrCCl_3$, thus indicating that O-rebound to the carbon radicals is very efficient (see Table S5). The HAT mechanism is further supported by the observed large deuterium isotope effects in the oxidation of [D_2]DHA, [D_{10}]ethylbenzene, and [D_8]toluene, with $k^H/k^D = 5.6$ (Figure 4b), 10 (see Figure S11), and 9.1 (see Figure S12), respectively. Similar linear correlations between $\log k'_2$ and C–H BDE were also observed in the oxidation of alkylaromatics by other metal oxo species such as $[Ru(O)(bpy)_2py]^{2+}$[17] and $[Ru(O)_2(N_2O_2)]^{2+}$.[18]

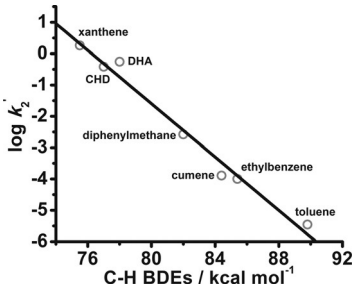

Figure 5. Plot of log k'_2 vs. C–H BDEs for the reaction between **$Os^{V}O$** and alkylaromatics in CH_3CN at 298.0 K. Slope = $-(4.26 \pm 0.26) \times 10^{-1}$; y-intercept = $(3.25 \pm 0.21) \times 10^1$; $r^2 = 0.9776$.

In conclusion, we have reported the first example of a group 8 seven-coordinate oxo species, $[Os^{V}(O)(qpy)(pic)Cl]^{2+}$. This complex readily undergoes O-atom transfer to phosphine and thioanisole, and H-atom transfer to alkylaromatics. Although a number of osmium(VI) dioxo species, such as $[Os(O)_2(TMC)]^{2+}$ (TMC = 1,4,8,11-tetramethyl-1,4,8,11-tetraazacyclotetradecane)[19] and *trans*-$[Os^{VI}(O)_2(4,4'\text{-}Me_2bipy)(CN)_2]$ (4,4′-Me_2bipy = 4,4′-dimethyl-2,2′-bipyridine)[20] are strong photooxidants, **$Os^{V}O$** can thermally abstract H atoms from alkylaromatics with C–H BDE as high as 90 kcal mol^{-1}, which to the best of our knowledge has not been reported for other osmium oxo species. Our work suggests that highly active oxidants may be designed based on group 8 seven-coordinate metal-oxo species.

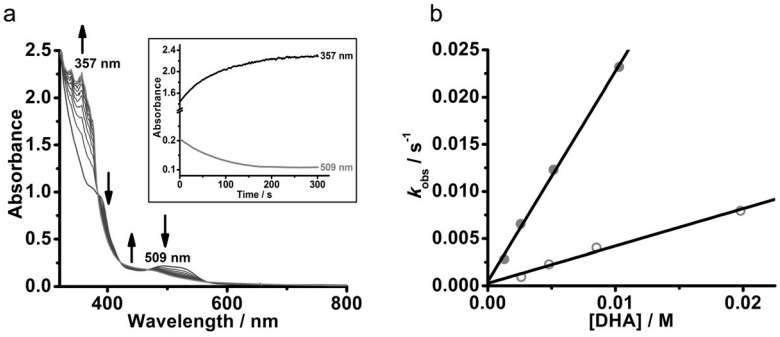

Figure 4. a) Spectral changes at 20 s intervals for the reaction between **$Os^{V}O$** (1.71×10^{-4} M) and DHA (5.15×10^{-3} M) in CH_3CN at 298.0 K. Inset shows the corresponding absorbance-time traces at 357 and 509 nm. b) Plot of k_{obs} vs. [DHA] for the reaction between **$Os^{V}O$** and DHA in CH_3CN at 298.0 K [for DHA (solid circle): slope = (2.23 ± 0.07); y-intercept = $(4.59 \pm 4.50) \times 10^{-4}$; $r^2 = 0.9965$. For [D_4]DHA (open circle): slope = $(3.95 \pm 0.31) \times 10^{-1}$; y-intercept = $(2.68 \pm 3.43) \times 10^{-4}$; $r^2 = 0.9819$]. KIE = (5.6 ± 1).

Acknowledgements

The work described in this paper was supported by Hong Kong University Grants Committee (AoE/P-03-08), the Research Grants Council of Hong Kong (CityU 101811), and the Shenzhen Science and Technology Research Grant (JCYJ20120613115247045).

Keywords: C–H activation · osmium · oxidation · structure elucidation · X-ray diffraction

How to cite: *Angew. Chem. Int. Ed.* **2016**, *55*, 288–291
Angew. Chem. **2016**, *128*, 296–299

[1] A. Gunay, K. H. Theopold, *Chem. Rev.* **2010**, *110*, 1060–1081.
[2] I. G. Denisov, T. M. Makris, S. G. Sligar, I. Schlichting, *Chem. Rev.* **2005**, *105*, 2253–2278.
[3] M. Costas, M. P. Mehn, M. P. Jensen, L. Que, Jr., *Chem. Rev.* **2004**, *104*, 939–986.
[4] I. Schlichting, J. Berendzen, K. Chu, A. M. Stock, S. A. Maves, D. E. Benson, R. M. Sweet, D. Ringe, G. A. Petsko, S. G. Sligar, *Science* **2000**, *287*, 1615–1622.
[5] a) W. Nam, *Acc. Chem. Res.* **2015**, *48*, 2415–2423; b) C.-W. Tse, T. W.-S. Chow, Z. Guo, H. K. Lee, J.-S. Huang, C.-M. Che, *Angew. Chem. Int. Ed.* **2014**, *53*, 798–803; *Angew. Chem.* **2014**, *126*, 817–822; c) L. Que, Jr., *Acc. Chem. Res.* **2007**, *40*, 493–500; d) C. Krebs, D. G. Fujimori, C. T. Walsh, J. M. Bollinger, *Acc. Chem. Res.* **2007**, *40*, 484–492; e) V. K. Sharma, R. Zboril, R. S. Varma, *Acc. Chem. Res.* **2015**, *48*, 182–191.
[6] a) W.-P. Yip, W.-Y. Yu, N. Zhu, C.-M. Che, *J. Am. Chem. Soc.* **2005**, *127*, 14239–14249; b) A. S. Goldstein, R. H. Beer, R. S. Drago, *J. Am. Chem. Soc.* **1994**, *116*, 2424–2429; c) T. Kojima, K. Nakayama, K. Ikemura, T. Ogura, S. Fukuzumi, *J. Am. Chem. Soc.* **2011**, *133*, 11692–11700; d) T. J. Meyer, M. H. V. Huynh, *Inorg. Chem.* **2003**, *42*, 8140–8160; e) W. P. Griffith, *Ruthenium Oxidation Complexes*, Springer, New York, **2011**.
[7] C.-M. Che, T.-C. Lau, *Comprehensive Coordination Chemistry II*, *Vol. 5*, Elsevier, Amsterdam, **2003**, pp. 733–847.
[8] a) H. C. Kolb, M. S. VanNieuwenhze, K. B. Sharpless, *Chem. Rev.* **1994**, *94*, 2483–2547; b) E. N. Jacobsen, I. Marko, W. S. Mungall, G. Schroeder, K. B. Sharpless, *J. Am. Chem. Soc.* **1988**, *110*, 1968–1970.
[9] a) H. Sugimoto, K. Kitayama, S. Mori, S. Itoh, *J. Am. Chem. Soc.* **2012**, *134*, 19270–19280; b) H. Sugimoto, K. Ashikari, S. Itoh, *Chem. Asian J.* **2013**, *8*, 2154–2160.
[10] a) H.-W. Tseng, R. Zong, J. T. Muckerman, R. Thummel, *Inorg. Chem.* **2008**, *47*, 11763–11773; b) J. T. Muckerman, M. Kowalczyk, Y. M. Badiei, D. E. Polyansky, J. J. Concepcion, R. Zong, R. P. Thummel, E. Fujita, *Inorg. Chem.* **2014**, *53*, 6904–6913.
[11] a) L. Duan, A. Fischer, Y. Xu, L. Sun, *J. Am. Chem. Soc.* **2009**, *131*, 10397–10399; b) L. Duan, F. Bozoglian, S. Mandal, B. Stewart, T. Privalov, A. Llobet, L. Sun, *Nat. Chem.* **2012**, *4*, 418–423.
[12] Y. Liu, S.-M. Ng, S.-M. Yiu, W. W. Y. Lam, X.-G. Wei, K.-C. Lau, T.-C. Lau, *Angew. Chem. Int. Ed.* **2014**, *53*, 14468–14471; *Angew. Chem.* **2014**, *126*, 14696–14699.
[13] T. Kojima, Y. Hirai, T. Ishizuka, Y. Shiota, K. Yoshizawa, K. Ikemura, T. Ogura, S. Fukuzumi, *Angew. Chem. Int. Ed.* **2010**, *49*, 8449–8453; *Angew. Chem.* **2010**, *122*, 8627–8631.
[14] S. Ohzu, T. Ishizuka, Y. Hirai, H. Jiang, M. Sakaguchi, T. Ogura, S. Fukuzumi, T. Kojima, *Chem. Sci.* **2012**, *3*, 3421–3431.
[15] T. Ishizuka, S. Ohzu, H. Kotani, Y. Shiota, K. Yoshizawa, T. Kojima, *Chem. Sci.* **2014**, *5*, 1429–1436.
[16] S. Shaik, D. Kumar, S. P. de Visser, A. Altun, W. Thiel, *Chem. Rev.* **2005**, *105*, 2279–2328.
[17] T. Matsuo, J. M. Mayer, *Inorg. Chem.* **2005**, *44*, 2150–2158.
[18] W. W. Y. Lam, W.-L. Man, Y.-N. Wang, T.-C. Lau, *Inorg. Chem.* **2008**, *47*, 6771–6778.
[19] a) C.-M. Che, W. Cheng, V. W.-W. Yam, *J. Chem. Soc. Dalton Trans.* **1990**, 3095–3100; b) S. Schindler, E. W. Castner, Jr., C. Creutz, N. Sutin, *Inorg. Chem.* **1993**, *32*, 4200–4208.
[20] K.-F. Chin, Y.-K. Cheng, K.-K. Cheung, C.-X. Guo, C.-M. Che, *J. Chem. Soc. Dalton Trans.* **1995**, 2967–2973.

Received: August 24, 2015
Revised: October 14, 2015
Published online: November 10, 2015

